Finite-Difference Viscous Filtering for Non-regular Meshes

R. Perrin, Eric Lamballais

Finite-difference viscous filtering for non-regular meshes

R. Perrin and E. Lamballais

1 Introduction

In a recent study [1], the authors have proposed a new solution filtering technique for direct and large-eddy simulation (DNS/LES). This method can represent both the molecular and artificial viscosity. It is particularly easy to code in a conventional finite-difference framework where only the scheme coefficients have to be designed to ensure the expected dissipation. The main strength of this *viscous filtering* technique lies in its numerical stability features. In this sense, it can be considered as a simple and computationally efficient alternative to implicit time integration of the viscous term.

The concept of viscous filtering and its advantages in the context of DNS/LES are presented in [1]. However, as a limitation of the technique, only the case of a regular mesh has been addressed. It was a way to design the coefficients for ensuring favourable spectral features defined in the Fourier space. In particular, the accuracy conditions are derived through Taylor's expansions expressed in wavenumbers.

The purpose of this contribution is to extend this viscous filtering technique to non-regular meshes. This generalization requires to express the expected features in the physical space in order to obtain the various relations to reach a given order of accuracy. The principles of these developments are first presented. Then, a preliminary validation is shown for the Burgers equation. Finally, to assess the method in a DNS/LES context, the case of a transitional boundary layer is considered with the use of a highly stretched mesh in the near-wall region.

R. Perrin
Department of Mechanical Engineering, Faculty of Engineering at Sriracha, Kasetsart University Sriracha Campus, Thailand, e-mail: rodolphe@eng.src.ku.ac.th

E. Lamballais
Curiosity Group, Pprime Institute, CNRS - Univ-Poitiers - ISAE/ENSMA, France, e-mail: eric.lamballais@univ-poitiers.fr

2 Methodology

To present the general ideas of the approach, let us consider the simple one-dimensional equation

$$\frac{\partial u}{\partial t} = F(u) + \nu \frac{\partial^2 u}{\partial x^2} \tag{1}$$

where $u(x,t)$ is the solution and ν the constant molecular viscosity. The basic principle of the method is to split the time advancement into two steps with

$$u^* = u^n + \int_{t_n}^{t_n+\Delta t} F(u)\, dt \tag{2}$$

$$u^{n+1} = \widetilde{u^*} \tag{3}$$

with $u^n = u(x,t_n)$ and $u^{n+1} = u(x,t_n+\Delta t)$. Step (2) consists in the time advancement of the inviscid version of equation (1) where the integral can be evaluated for instance by an Adams-Bashforth scheme. Step (3) corresponds to the application of a spatial filter denoted $\widetilde{.}$ to restore the influence of viscosity. For simplicity, the splitting error is ignored here, but it has been shown in [1] that this error is negligible for typical DNS/LES while being removable if necessary.

The spatial discretization is based on a stretched mesh $x_i = h(s_i)$ where $s_i = (i-1)\Delta s$ corresponds to regularly distributed nodes on the computational coordinate s. This coordinate transformation enables to write successive derivatives as

$$\begin{aligned} &\frac{\partial u}{\partial x} = g\frac{\partial u}{\partial s} \quad , \quad \frac{\partial^2 u}{\partial x^2} = g^2\frac{\partial^2 u}{\partial s^2} + gg'\frac{\partial u}{\partial s} \\ &\frac{\partial^3 u}{\partial x^3} = g^3\frac{\partial^3 u}{\partial s^3} + 3g^2g'\frac{\partial^2 u}{\partial s^2} + \left(g^2g^{(2)} + gg'^2\right)\frac{\partial u}{\partial s} \quad , \quad \frac{\partial^n u}{\partial x^n} = g^n\frac{\partial^n u}{\partial s^n} + \ldots \end{aligned} \tag{4}$$

where $g = 1/h'$. To mimic the contribution of this viscous term in step (3), a finite-difference filter scheme of the form

$$\alpha_p\tilde{u}_{i+1} + \tilde{u}_i + \alpha_m\tilde{u}_{i-1} = au_i + \frac{b_p}{2}u_{i+1} + \frac{b_m}{2}u_{i-1} + \frac{c_p}{2}u_{i+2} + \frac{c_m}{2}u_{i-2} \tag{5}$$

is used where $u_i = u(x_i,t)$. As it is usual in a finite-difference framework, Taylor's expansion in space

$$\begin{aligned} u_{i+k} &= u_i + \sum_{p=1}^{n} \frac{(k\Delta s)^p}{p!} \left.\frac{\partial^p u}{\partial s^p}\right|_i + O(\Delta s^{n+1}) \\ \left.\frac{\partial^q u}{\partial s^q}\right|_{i+k} &= \left.\frac{\partial^q u}{\partial s^q}\right|_i + \sum_{p=1}^{n} \frac{(k\Delta s)^p}{p!} \left.\frac{\partial^{p+q} u}{\partial s^{p+q}}\right|_i + O(\Delta s^{n+1}) \end{aligned} \tag{6}$$

provides relation orders in Δs^n between the coefficients $(\alpha_p, \alpha_m, a, b_p, b_m, c_p, c_m)$ in (5). Then, by Taylor's expansion in time

$$\tilde{u}_i = u_i + \Delta t \left.\frac{\partial u}{\partial t}\right|_i + \frac{\Delta t^2}{2} \left.\frac{\partial^2 u}{\partial t^2}\right|_i + \frac{\Delta t^3}{3!} \left.\frac{\partial^3 u}{\partial t^3}\right|_i + O(\Delta t^4) \tag{7}$$

while switching the time derivative by their spatial counterparts, requiring that step (3) has to match a purely diffusive equation with

$$\frac{\partial u}{\partial t} = \nu \frac{\partial^2 u}{\partial x^2} \quad , \quad \frac{\partial^2 u}{\partial t^2} = \nu^2 \frac{\partial^4 u}{\partial x^4} \quad , \quad \frac{\partial^3 u}{\partial t^3} = \nu^3 \frac{\partial^6 u}{\partial x^6}, \tag{8}$$

expansion (7) can also be written as

$$\tilde{u}_i = u_i + F\Delta s^2 \left.\frac{\partial^2 u}{\partial x^2}\right|_i + \frac{F^2\Delta s^4}{2} \left.\frac{\partial^4 u}{\partial x^4}\right|_i + \frac{F^3\Delta s^6}{3!} \left.\frac{\partial^6 u}{\partial x^6}\right|_i + O(F^4\Delta x^8) \tag{9}$$

where $F = \frac{\nu\Delta t}{\Delta s^2}$ is the Fourier number based on the constant cell Δs. To enable an identification between the relation orders given by (6) and (9) in the scheme (5), a conversion of the spatial derivatives from x to s is required. This can be done easily through relations (4) so that a 7×7 system $MX = N$ can be obtained where the component of $X = (\alpha_p, \alpha_m, a, b_p, b_m, c_p, c_m)^T$ are the unknown scheme coefficients of (5). This system can be solved analytically (using a symbolic calculation tool) leading to extremely long expressions for each coefficient which is a function of F, g, g', g'', $g^{(3)}$, $g^{(4)}$ and $g^{(5)}$. More conveniently, the same can be done numerically up to the machine accuracy before starting the simulation.

Specific versions of this new scheme have also been developed for performing implicit LES. In that case, an artificial dissipation can be imposed by checking

$$a - \frac{b_p}{2} - \frac{b_m}{2} + \frac{c_p}{2} + \frac{c_m}{2} - d = (1 - \alpha_p - \alpha_m) \exp\left[-\pi^2 \left(\frac{\nu_0}{\nu} + 1\right) g^2 F\right] \tag{10}$$

where $d = d_p = d_m$ is a stencil extension of the initial scheme (5) while ν_0 is a numerical viscosity chosen to ensure regularization as a substitute of subgrid-scale modelling. The resulting 8×8 system can be solved as previously, leading to scheme coefficients with an extra dependency on ν_0.

Finally, the same methodology can be straightforwardly followed for the development of one-sided schemes at the boundaries.

3 Validation for Burger's equation

To validate this new type of filter scheme, Burgers' equation has been solved, namely $F(u) = u\partial u/\partial x$ in (1). As explained in the previous section, every time step, the inviscid Burger equation is solved and then, the viscous filter scheme (5) is applied on the discrete solution to restore the influence of the viscosity. A time interval after the shock formation is computed and the solution is compared to its exact counterpart. The mesh, composed of N nodes, is regular when using the initial scheme given in [1] whereas the mesh is stretched in the shock region when using

the new scheme developed here. The sixth-order version is assessed, namely the highest-order enabled by scheme (5) because of its compact stencil.

As expected, at low resolution using a regular mesh, the solution is subjected to Gibbs' phenomenon, leading to unphysical grid-to-grid oscillations in the near-shock region as exhibited in figure 1-left. This problem can be fixed through the increase of the resolution everywhere in the domain, which is computationally inefficient. Alternatively, the use of a stretched grid enables us to remove the unphysical oscillations without any increase of the computational cost (see figure 1-left for $N = 64$).

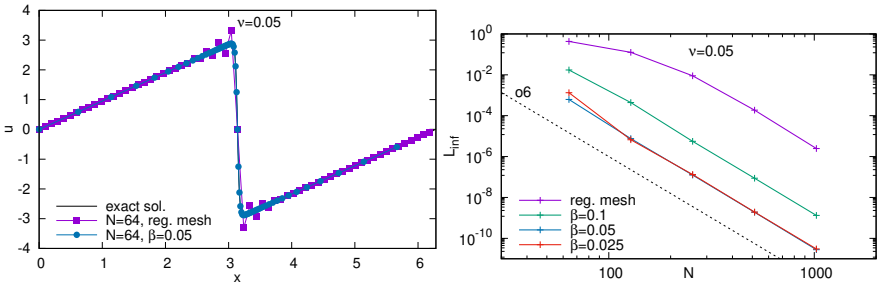

Fig. 1 Computation of a shocked Burgers' solution. Top: solution at $t = 0.05$. Bottom: evolution of L_∞ with the number N of mesh nodes.

The numerical convergence analysis is based on the computation of L_∞ to estimate the numerical error defined by reference to the exact solution. Figure 1-right shows that the expected sixth-order is correctly recovered for both the regular and non-regular meshes, but only at high resolution for the former as the signature of the Gibbs phenomenon at low resolution. The spectacular increase of the accuracy provided by the use of a stretched mesh can be observed, with for the two largest stretching parameters $\beta = (0.05, 0.025)$, a reduction by more than 2 orders of magnitude of the maximum error located near the shock. For a constant error, the computational saving corresponds to a factor of about 8 by comparison to a regular mesh.

4 Assessment by implicit LES

For further validation, implicit LES of a spatially-evolving boundary layer subjected to bypass transition has been carried out as in [2]. To handle the present flow configuration, a Cartesian mesh of $(n_x \times n_y \times n_z) = (961, 411, 156)$ nodes is used to cover a computational domain $(L_x \times L_y \times L_z) = (1500\delta_1, 145\delta_1, 125\delta_1)$ where δ_1 is the displacement thickness of the laminar boundary layer at the inlet of the computational domain and $Re = U_0\delta_1/\nu = 300$. The inlet boundary conditions are provided by precursor simulations in which the flow in the leading edge region of the flat

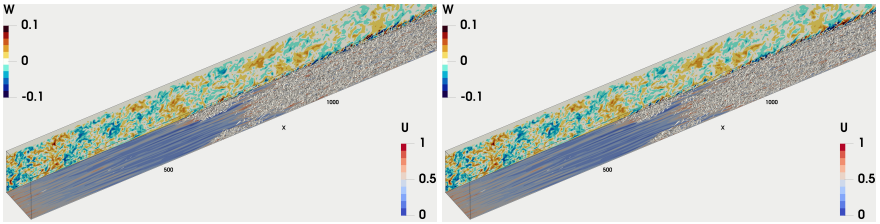

Fig. 2 Implicit LES of bypass transition of a boundary layer [2]. Maps of longitudinal and spanwise velocities at $y = \delta_1$ and $z = \delta_1$ respectively. Q-criterion isosurface in grey.

plate is computed together with realistic free-stream turbulence outside the boundary layer in order to trigger physically relevant bypass transition (see [2] for more details). Based on the maximum friction velocity u_τ, the resulting cell sizes in wall-units are $(\Delta x^+, \Delta y^+, \Delta z^+) \approx (23, 1-27, 12)$ through the use of a highly stretched mesh in the wall-normal direction y. The near-wall cell-size $\Delta y^+ \approx 1$ is favourable for accuracy but penalizing for numerical stability when using an explicit time advancement, in particular for the high value of numerical viscosity used here with $\nu_0/\nu = 25$. For the present second-order Adams-Bashforth (AB2) scheme, numerical stability is ensured only if the maximum Fourier number $F_{\max} = \nu\Delta t/\Delta_{\min}^2$ is less than $3.9\,10^{-3}$, imposing the use of a time step Δt reduced by a factor 18 by comparison to its maximum value allowed by the CFL condition. To alleviate this problem, the traditional approach is to make implicit the time integration of the viscous term using for instance a Crank-Nicolson (CN) scheme, leading to an hybrid AB2-CN time advancement. Here, the present viscous filtering (VF) technique is proposed as a simpler alternative designated as AB2-VF.

It has been observed that both AB2-CN and AB2-VF strategies enable the use of large time steps only restricted by the CFL condition while leading to virtually identical instantaneous solutions as illustrated in figure 2 where significant differences are only observed in flow regions where the dynamics becomes chaotic. This point can be confirmed by plotting time signals of velocity as shown in figure 3 for deterministic (top-left) and intermitently chaotic (top-right) boundary-layer regions. In the free-stream turbulence zone, the agreement is almost perfect up to the most downstream region because of the low level of velocity fluctuations with respect to the convection velocity U_0. Similar agreements are observed for other quantities (not shown for brevity) leading to the conclusion that AB2-CN and AB2-VF strategies are equivalent in terms of numerical accuracy and stability.

5 Conclusion

The main conclusion of these one-dimensional and full-scale tests is that viscous filtering can be extended to non-regular meshes while ensuring accuracy and quasi-

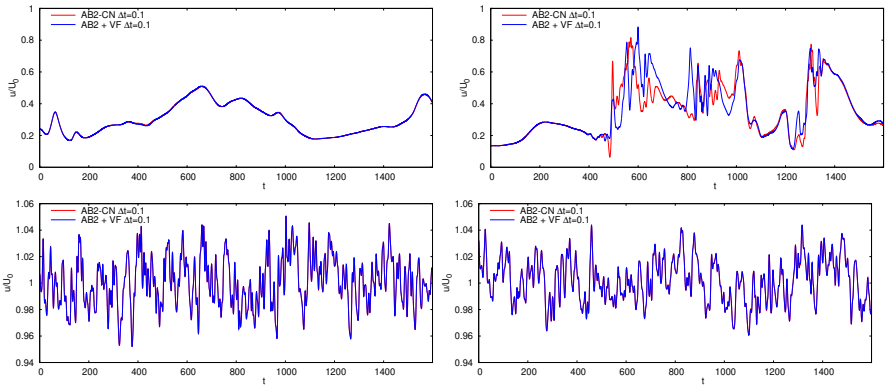

Fig. 3 Time signals of the longitudinal velocity at $(x,y) = (400\delta_1, 0.8\delta_1, 50\delta_1)$ left-top, $(x,y) = (700\delta_1, 0.8\delta_1)$ right-top, $(x,y) = (400\delta_1)$ left-bottom, $(x,y) = (700\delta_1)$ right-bottom with $z = 50\delta_1$.

unconditional stability, as a valuable alternative to an implicit treatment of the viscous term in time. By comparison to the latter, viscous filtering can easily handle multidimensional problems thanks to its essentially explicit nature based on operator splitting. In particular, it does not require the use of sophisticated and iterative methods to deal with large-size and sparse matrices while enabling the use of large time steps not restricted by viscous numerical stability conditions. Among the perspectives of the present approach, one may refer to an adaptation for flows with variable viscosity in space. The extension of the present concept of viscous filtering to other frameworks of numerical methods such as finite volume/element would also deserve further developements.

6 Acknowledgements

This work was granted access to the HPC resources of IDRIS under the allocation A0072A07624 made by GENCI.

References

1. E. Lamballais, R. Vicente Cruz and R. Perrin, “Viscous and hyperviscous filtering for direct and large-eddy simulation”, *J. Comp. Phys.*, vol. 431, p. 110115, 2021.
2. R. Perrin and E. Lamballais, “Assessment of implicit LES modelling for bypass transition of a boundary layer”, *Computers and Fluids*, vol. 251, 105728, 2022.